



**HAL**  
open science

## Thermo-mechanical calculation of printed circuit heat exchanger using homogenization

Christophe Garnier, Sébastien Vincent, Pierre Lamagnere, Yves Lejeail, Lionel Cachon

► **To cite this version:**

Christophe Garnier, Sébastien Vincent, Pierre Lamagnere, Yves Lejeail, Lionel Cachon. Thermo-mechanical calculation of printed circuit heat exchanger using homogenization. *Journal of Thermal Science*, In press, 10.1007/s11630-022-1646-1 . cea-03714046

**HAL Id: cea-03714046**

**<https://cea.hal.science/cea-03714046>**

Submitted on 5 Jul 2022

**HAL** is a multi-disciplinary open access archive for the deposit and dissemination of scientific research documents, whether they are published or not. The documents may come from teaching and research institutions in France or abroad, or from public or private research centers.

L'archive ouverte pluridisciplinaire **HAL**, est destinée au dépôt et à la diffusion de documents scientifiques de niveau recherche, publiés ou non, émanant des établissements d'enseignement et de recherche français ou étrangers, des laboratoires publics ou privés.

# Thermo-mechanical calculation of Printed Circuit Heat Exchanger using homogenization

**GARNIER Christophe**<sup>1\*</sup>, **VINCENT Sébastien**<sup>1</sup>, **LAMAGNERE Pierre**<sup>1</sup>, **LEJEAIL Yves**<sup>1</sup>, **CACHON Lionel**<sup>1</sup>

1. CEA, DES, IRESNE, Nuclear Technology Department, Cadarache F-13108 Saint-Paul-Lez-Durance, France.

**Corresponding author: GARNIER Christophe**

**E-mail: christophe.garnier@cea.fr**

## Abstract

The Finite-Element Method (FEM) is mainly used to design Compact Heat Exchanger structures. However, the narrow channel structures require fine mesh to accurately compute stress and strain. Combined with the dimensions of the overall component, this leads to an excessively large numerical model and therefore long computing times. This is especially true for transient thermal analyses, which require taking into account the full geometry. It is therefore interesting to reduce the size of the mesh. Periodic homogenization is an efficient method for achieving this goal. It can be applied to the core of the structure when periodic patterns (identified on basis of the arrangement of the channels) exist. A method based on this technique, with some improvements, is proposed in this paper for thermal loading without internal pressure. In addition to the Equivalent Homogenous Medium (EHM) replacing the periodic patterns, some explicit channels are interposed between the EHM and the cover plates. This has two advantages. The first is to smooth the transition of stiffness between the cover plates and the homogenized medium. The second one is to be able to directly compute stress and strain on the most critical channels located in this area. This paper assesses the method's effectiveness for thermal loadings in order to conduct thermal stress analyses. First, the equivalent elastic constants of the EHM are obtained with a numerical Finite Elements Method. Then, two 2D cases using EHM are compared against a 2D explicit model (*i.e.* explicit geometry for the core channels). These cases are chosen to validate the EHM itself and its effectiveness for a real section of the heat exchanger. Results show very good agreement with a relative difference lower than 1 %. In addition, the sensitivity to the number of layers added between the EHM and the cover plates is analysed. It is recommended interposing at least two layers of patterns to obtain converged results for the considered configuration. Finally, a triangular mesh is considered to reduce the size of the model. No difference with a regular quadrangular mesh can be observed whereas the computing time is reduced. This method can be used to perform the design of any CHE under thermal loading as long as the channel arrangement shows periodicity.

## Keywords

Compact Heat Exchanger, Thermal stress, Finite Element Method, Homogenization.

## 1 Introduction

Compact Heat Exchanger (CHE) are considered for various applications that need to be compact for effective heat transfers. The nuclear industry, and particularly Generation IV reactors, uses such heat exchanger technologies. Various reactor types can benefit from the development of such technologies

(e.g. see [1,4]). The CEA designed a concept with this technology for its Sodium Fast Reactor (SFR) project, called ASTRID (see [5,7]). In this application, the Brayton cycle option with gas (nitrogen) as coolant is foreseen for the tertiary loop. A CHE with Printed Circuit Heat Exchanger technology (PCHE) is used to transfer the heat between the sodium secondary loop and the gas tertiary loop. PCHEs are composed of multiple plates integrating flow channels. These plates are generally assembled with a diffusion bonding technology.

Even though CHEs are extremely compact compared with shell and tube Heat Exchangers (HE), the large amount of heat to be transferred from the hot side to the cold side in nuclear applications requires implementing numerous channels. Moreover, the high level of nuclear requirements entails strong design substantiation, particularly the mechanical design for safety-classified components. This requires computing the stress and strain resulting from the various loads (static or transient) that can occur, either with elastic or inelastic analysis. Analytical models are limited and not accurate enough, which is why numerical tools such as Finite-Element Method (FEM) are mainly used. However, the narrow channel structures require a fine mesh to accurately compute stress and strain. This, combined with the size of the overall component, leads to an excessively large numerical model, particularly for transient thermal analyses, which require taking into account the full size of the geometry. Consequently, alternative modelling methods to full-scale techniques and explicit geometry are required. In this paper, a new method based on usual homogenization models is presented in order to compute local strain and stress values in CHE with a reduced number of nodes. The main improvement of the method is to insert some layers of channels with explicit geometry between homogenous medium (core of the HE) and the other parts of the HE. The stress and strain can then be directly computed on this intermediate layer which is found to be a critical area of the HE.

The homogenization method is relevant for reducing the size of the numerical model. Furthermore, its application to CHEs can take advantage of the periodicity of the channel arrangement to apply the specific theory of periodic homogenization either to 2D or 3D problems.

Globally, CHE design methods (not necessarily restricted to nuclear applications) are classified according to the scale of analysis: either local analysis that is generally used in parametric studies (geometric or loading effects), or a global model that is used to design CHEs with representative loads. The thermal loading is generally computed separately and then imported into the mechanical model.

Due to the limited scale of the geometry, a local analysis can use a fine mesh and can model an explicit detailed geometry. However, the applied boundary conditions must represent the overall behaviour of the section. Yet, this cannot be achieved without actually knowing the overall behaviour of the section, which implies using the full geometry. Therefore, simplified boundary conditions are generally applied and 2D assumption can also be considered.

Simanjuntak and Lee [8] describe an elastic static local model with an explicit 2D geometry in order to analyse the impact of channel misalignment through parametric studies. Their boundary conditions are symmetry and periodic load conditions. The resulting mesh comprises 10,705 elements, which can be considered as small thanks to 2D modelling.

Lee and Lee [9] assess a PCHE with a local static pseudo-explicit 2D model (thickness of 0.1 mm, no load variation in the thickness). This model aims at computing stress and strain on several explicit channels in order to evaluate their compliance with the design criteria recommended in the ASME code (American Society of Mechanical Engineers, part Boiler and Pressure Vessel Code, Section III). Elastic and inelastic models are both used. Loads are the internal pressure and the thermal loading. Unconstrained boundary conditions are applied (a weak spring is added to the side to prevent rigid body motion), leading to a plane strain model that overestimates stress. As a consequence, a sensitivity analysis on both PCHE channel numbers (3 configurations from  $2 \times 1$  to  $8 \times 8$  channels) and element sizes (from  $2.50 \cdot 10^{-5}$  m to  $5.00 \cdot 10^{-3}$  m) is conducted. It aims at defining the minimum number of PCHE channels for modelling representative stress fields around selected hot and cold channels. These channels are considered as reference units and are used for the mechanical analysis. It is found that the  $4 \times 4$  and  $8 \times 8$  configurations are the most accurate, especially to compute stress around the channels

ends, since they both lead to nearly the same results. The results are also compared with analytical formulas, which are found to underestimate the numerically calculated stress intensities. The 4×4 configuration contains up to 689,980 elements whereas the 8×8 configuration has up to 1,222,619 elements.

Similarly, de la Torre *et al.* [10] describes an analysis with a plastic behaviour model and parametric study on both geometric parameters and thermal gradients. As for Lee and Lee [9], the influence of both the number of channels (from 2×1 to 12×7) and the mesh size are analysed since unrestrained support is used as boundary conditions. The configuration with 8×5 channels is retained for further analysis of the reference unit cell. The results are also compared with analytical formulas for simple geometry (hollow cylinder, plane stress). It has been found that these formulas can be used for preliminary design. The mesh contains up to 451,670 elements and 2,108,195 nodes for the 12×7 channels.

The previous examples show that even though the size of the model with only a few channels is relatively reduced compared with the full size of a HE, a high number of elements is nonetheless required. Moreover, the geometries essentially concern channels, they do not take into account the effect of cover plates, and analyses are mainly static.

Methods using global models involve larger-scale models and set out to evaluate the overall behaviour of the component, generally with 3D geometry. Park *et al.* [11] describe the design of a steam generator with straight tubes. Axisymmetric elements are used whenever possible. No information is given on the mesh. A transient analysis is also performed. Wu *et al.* [12] present the analysis results of a full-scale 3D model of the core including the cover plates of a PCHE. It contains 80 channels that are 713 mm in length. Although this is a relatively reduced geometry with only a limited number of channels, the resulting mesh involves 1.68 million nodes and 1.55 million elements. A static elastic analysis is performed. It is observed that a 3D global structure model can avoid calculation error caused by a local structural model that only contains partial periodic heat transfer channels. These examples show that a large number of nodes is required to analyse a full-scale model and computation times can be very long or prohibitive especially for transient analysis.

The homogenization method is relevant for reducing the size of the numerical model. The homogenization theory (see [13]) models the macroscopic behaviour of any media on basis of its microscopic characteristics (multiscale approach). It is used to model microstructures (see [14,15]), porous media and powders (see [16,18]), as well as periodic media (see [19,21]). Among them, composite media is one of the most common applications, used either to model the composite itself or composite structures with geometrical periodicities (see [22,24]). It has also been applied in the nuclear research sector, such as on fuels ([25]) or cladding for fast reactors ([26,28]).

In the field of HEs and CHEs, application of the homogenization method is investigated for the overall design of the full-scale component, with either elastic or plastic models. It can be efficiently coupled with FEM as illustrated in the following examples.

A first step of the method consists in identifying the homogenized elastic constants. Ge *et al.* [29] detail an analytical method used to compute these coefficients for Plate-Fin Heat Exchangers (PFHE) and without the effect of internal pressure. They are found to be anisotropic due to the geometry. FEM is also largely used to compute the homogenized elastic constants for periodic structures. The method is based on the periodic homogenization theory (see [13]) and has different formulations (see [25]). Xu and Qiao [30] provide the analytical results for a honeycomb sandwich that are validated with FEM. Dirrenberger and Forest [31] present the results for the homogenized elastic constants of two periodic structures using three methods which lead to equal results. In Tsuda *et al.* [32], a numerical method using FEM is set up to determine homogenized elastic-viscoplastic constants and macro stresses for PFHE taking into account the effect of the internal pressure, which is found to modify the homogenized constants. This model is validated through a comparison with a detailed FEM analysis including the internal pressure. This approach is then improved with a “duplex” model presented in [33] in which the fins and plates are homogenized separately. This results in two macroscopic constitutive models with improved accuracy in the results.

Mizokami *et al.* [34] propose a design procedure for PFHE using the homogenization method and taking into account creep damage. Stress or strain magnification factors are used to predict local stress and strain in the fin. In this approach, these factors can be defined as the ratio between the values of either the stress or the strain of the real structure and the ones of the equivalent solid. They are determined on the basis of the test results. The procedure is validated with pressure burst and thermal fatigue tests. The model takes into account the core (with equivalent homogeneous-solid model representative of Plates and Fins), straight fin area and headers. Finally, the method is used to design PFHEs with prediction of their creep-fatigue life by carrying out elastic and inelastic FEM analyses.

Ge *et al.* [35] use the above methodology to design a PFHE under pressure (primary stress analysis) and thermal stress loadings (including a transient analysis for the creep fatigue design). In addition to the method, they also use the above mentioned analytical relations concerning the homogenized elastic constants (see [29]), completed with equivalent thermophysical properties. The thermal stress model is elastic and uses an equivalent homogenous medium (EHM) to model the core. The full-scale geometry includes the equivalent core (size  $0.58 \times 0.42 \times 0.43 \text{ m}^3$ ), the headers and the straight fin area. It contains 34,130 nodes and 28,152 elements. This set of different elements leads to a design method and has been patented by Jiang *et al.* [36].

Finally, the method can also be used for dynamic modelling as shown by Planel and Brisson [37] with prediction of the dynamic behaviour of brazed HEs (fins separated with tubes).

Table 1 synthesizes the different approaches presented above with their advantages and drawbacks.

*Table 1: different types of thermomechanical calculations technics for heat exchangers*

Method	Geometry	Advantages	Drawbacks/limitations	References	Size of the model
Local analysis	Detailed explicit geometry, fine mesh	Accurate results, Plastic behaviour can be modelled	Simplified boundary conditions and loadings	[8]	10,705 elements
				[9] (PCHE)	Up to 1,222,619 elements
				[10]	Up to 451,670 elements
Global analysis	Explicit geometry	Representative loadings and boundary conditions	High number of elements, need of simplifications or components with reduced size	[11] (straight tubes)	Simplification of the geometry
				[12] (PCHE)	1.55 million elements
Global analysis with reduction technics	Homogenization method for periodic components (channels) Explicit geometry for other components	Reduction of the mesh size, representative loadings and boundary conditions	No explicit stress results for homogenized medium: need of relations between homogenous results and explicit geometry Sudden transition of physical properties between homogenous model and explicit components Plastic behaviour more difficult to model	[34] (PFHE)	No information
				[35] (PFHE)	28,152 elements
				[36] (patent, PFHE)	-
				[37] (fins separated with tubes)	No information

In this paper, an improvement of the periodic homogenization method is proposed for CHEs under pure thermal loading. The objective is to compute the resulting elastic thermal stress in order to design the component. However, the transition between the homogenous medium and real (*i.e.* explicit) parts of

the HE has proven to induce discontinuities in terms of stress. This region is most often considered as a critical part for the design of the HE so that accurate results are required. Therefore, the standard homogenization method is here modified since micro-macro relations are not applied. Instead, the FE model includes layers composed of the explicit geometry of the channels between the homogenized medium and the cover plates. This has two advantages. The first is to smooth the transition of stiffness between the cover plates and the homogenized medium. The second is to be able to directly compute the stress and strain on channels located in this area, channels which have been found to be the most critical (for example, see [12]). For the considered application, the internal pressure is disregarded and behaviour is elastic (elastic-equivalent constants are used). The specific case of 2D thermal loading is considered (simplified loading with applied temperatures and conduction through structures). Thus, 2D mechanical model is used to compute thermal stress using the generalized plain strains assumption. The periodic homogenization theory is applied to represent the HE core with its periodic channels with some specificities. The equivalent elastic constants of the medium representing the core are obtained with a numerical method using FEM.

In the present paper, the method is presented and assessed for a specific 2D PCHE pattern. However, it can be applied to any kind of CHE as long as the channel arrangement shows periodicity. The present article does not aim at designing the HE, so that results (displacement and stress) are not analysed according to any design code requirements, but only used for comparison purposes. However, in practice, they can be directly used to perform design analysis.

## 2 Method with Equivalent Homogenous Media

This section describes the overall method and its successive steps. It then briefly explains how the equivalent elastic constants are determined with FEM. These constants are used as model parameters for the overall method.

### 2.1 Description of the method

Periodic homogenization (see [13]) can be used for HE core in which periodic geometry is observed. It is coupled with FEM.

As previously said, it is proposed here to modify the standard method with additional layers composed of the explicit geometry of the channels between the homogenized medium and the cover plates. The stress on these channels can be directly computed.

Figure 1 presents the four steps of the method.

The first step consists in defining the input data for the method. This data includes the EHM constants, *i.e.* the equivalent elastic constants and the orthotropic thermal expansion coefficient. These parameters can be determined with the method using FEM, which is described in Sub-section 2.2.

The other input data is the temperature field of the EHM. As the thermal loading is taken into account, the temperature of the EHM must be computed. However, it is not possible to directly apply the explicit thermal loads to the EHM; explicit thermal loads should be applied to explicit geometry. Mizokami *et al.* [34] use a linear distribution from the low temperature inlet to the high temperature outlet (3D model), which results in a uniform mean temperature across the section. In Ge *et al.* [35], the temperature of the EHM is set according to the average temperature of the hot and cold gas and is considered constant across the cross section. In this paper, a periodic thermal loading is considered on the patterns. The explicit loading of the EHM is replaced by mean temperature of the pattern. It is computed separately using a dedicated thermal model with an explicit pattern, either in a static or transient analysis. The FEM thermal model described in Sub-section 2.2, which computes the equivalent thermal expansion coefficient, can be used in the case of static loading. Explicit thermal loading can be applied in this model. Periodic thermal loading results in a uniform mean temperature across the section. In the case of variable temperature across the section, the mean temperature of each pattern can be computed and described through a spatial profile.

The second step consists in establishing the thermal field of the whole geometry using a thermal model. The previously established temperature field can be applied directly to all EHM nodes, whereas explicit thermal loading can be applied to the other explicit part of the geometry. As the EHM temperature field is applied to the EHM nodes, thermal equilibrium does not have to be established for this part. Therefore, the equivalent thermophysical properties such as thermal conductivity, or the specific heat and density for transient thermal analysis are not required for the EHM with this method.

The third step uses the previous calculated thermal field as the nodal thermal load applied to a mechanical model. The mechanical boundary conditions complete the loading and the model can be solved.

Finally, the resulting mechanical quantities such as displacement, stress and strain are post-processed (step 4). Stress and strain can be either directly determined using explicit geometry (intermediate layer and cover plates) or by using classical micro-macro relations for EHM.

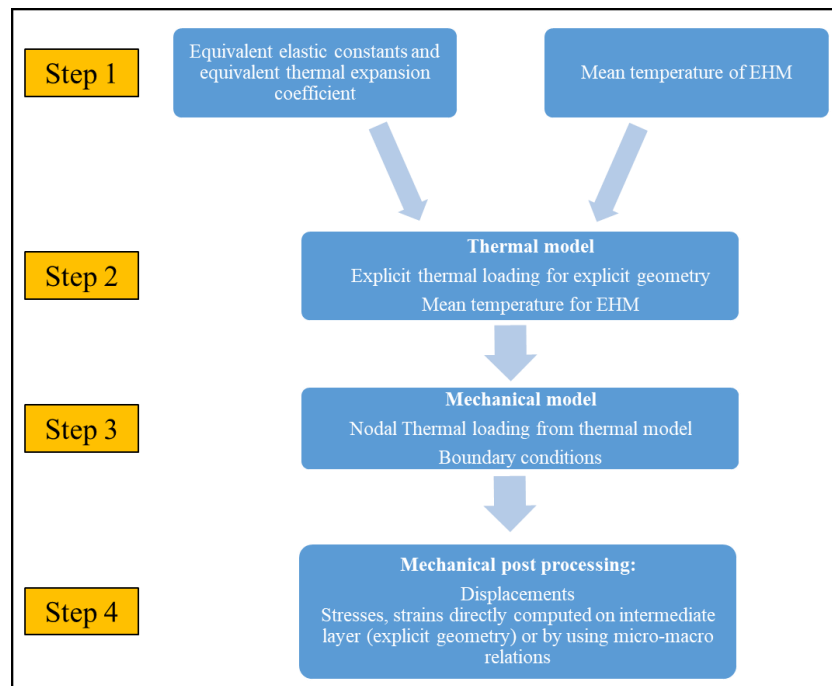


Figure 1: Method used to compute stress and strain with EHM

In this paper, this method using EHM is validated by comparing results of displacement and equivalent stress with explicit geometry simulations. A reduced 2D but representative section of the PCHE is considered. Its validation for any size of the section (2D) is discussed in Part 4. Figure 2 depicts the geometry of the finite-element model, including the explicit representative section shown in figure 2.a. The core is made up of periodic channels surrounded by cover plates. For the specific case in question, the fluids used are sodium and gas (nitrogen), which is why the channels are identified as sodium channels (“s”) and gas channels (“g”).

The pattern or unit cell can be defined on basis of the periodicity, which contains gas and sodium channels. It represents the unit cell or Representative Elementary Volume (REV), as shown in figure 2.b for the case in question. It is used to set up the EHM. Multiple geometries can be considered for the REV. This particular geometry has been selected on basis of geometric symmetrical planes which induce additional constraint relations on the boundaries of the pattern.

Figure 2.c shows the associated geometry using EHM to represent the core as well as the intermediate layer with explicit geometry. In this case, the intermediate layer contains two layers of explicit patterns. The accuracy of the results depends on the number of pattern layers for the intermediate explicit geometry. This parameter is analysed in Part 3.4.

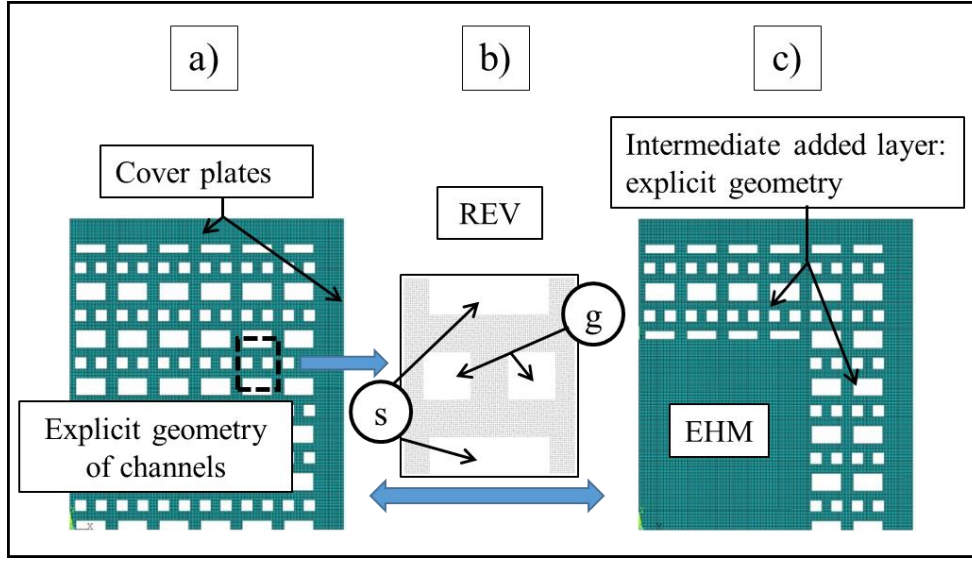


Figure 2: Geometry of the Finite-Element model with meshing (1/4 of CHE section) - a) Explicit geometry with 6x6 patterns, b) One pattern (equal to the REV) for the core channels, c) Equivalent geometry with EHM

The next subsection briefly describes the method used to compute the equivalent elastic constants of the EHM.

## 2.2 Determining the equivalent elastic constants with FEM

Equivalent elastic constants are computed using FEM. In the specific case in question, these are mechanical constants (elastic moduli in traction-compression, shear moduli, Poisson's ratios) and the thermal expansion coefficient.

They are based on isotropic material properties which are  $E_0$ , Young's modulus,  $\nu_0$ , Poisson's ratio and  $\alpha_0$ , the thermal expansion coefficient.

A first method is used to compute the mechanical constants.

Given the geometry of the REV (see figure 2.b), the behaviour is known to be orthotropic with the following equivalent elastic constants: moduli in traction-compression ( $E_x, E_y, E_z$ ), shear moduli ( $G_{xy}, G_{zx}, G_{zy}$ ) and Poisson's ratios ( $\nu_{xy}, \nu_{yz}, \nu_{xz}$ ). The expression of Hooke's elastic law is recalled in equation (1).

$$\begin{bmatrix} \varepsilon_x \\ \varepsilon_y \\ \varepsilon_z \\ \gamma_{xy} \\ \gamma_{xz} \\ \gamma_{yz} \end{bmatrix} = \begin{bmatrix} 1/E_x & -\nu_{xy}/E_x & -\nu_{xz}/E_x & 0 & 0 & 0 \\ -\nu_{yx}/E_y & 1/E_y & -\nu_{yz}/E_y & 0 & 0 & 0 \\ -\nu_{zx}/E_z & -\nu_{zy}/E_z & 1/E_z & 0 & 0 & 0 \\ 0 & 0 & 0 & 1/G_{xy} & 0 & 0 \\ 0 & 0 & 0 & 0 & 1/G_{xz} & 0 \\ 0 & 0 & 0 & 0 & 0 & 1/G_{yz} \end{bmatrix} \begin{bmatrix} \sigma_x \\ \sigma_y \\ \sigma_z \\ \tau_{xy} \\ \tau_{xz} \\ \tau_{yz} \end{bmatrix} \quad (1)$$

with:  $\gamma_{xy}=2 \varepsilon_{xy}, \gamma_{xz}=2 \varepsilon_{xz}, \gamma_{yz}=2 \varepsilon_{yz}$

The homogenization method aims at computing the previous equivalent elastic constants for the considered REV.

The FEM model, together with the associated boundary conditions and loadings, are based on the periodic homogenization theory (see [13] and [25]). The “mechanic” approach is used as defined in di Paola [25]. The homogenous boundary conditions are based on periodic formulation according to the Hill condition. They had to comply with the following relation:

$$\begin{aligned} \mathbf{u}(\mathbf{x}) &= \mathbf{E}^0 \mathbf{x} + \mathbf{u}'(\mathbf{x}) \quad \forall \mathbf{x} \in \partial V \\ \text{div}(\boldsymbol{\sigma}(\mathbf{x})) &= 0 \end{aligned} \quad (2)$$

with:

$\partial V$  the edges of the volume  $V$ ,

$\mathbf{u}(\mathbf{x})$  a displacement vector imposed on the edges of the volume (with  $\mathbf{x}$  the coordinates (vector) of any point of the edge),

$\mathbf{E}^0$  a macroscopic homogenous strain (tensor),  $\boldsymbol{\sigma}$  the stress tensor,

$\mathbf{u}'(\mathbf{x})$  must be the periodic displacement vector field, meaning that it has the same value for homologous points of  $\partial V$  (i.e. with  $\mathbf{L}$  the periodicity (vector),  $\mathbf{x}_1$  and  $\mathbf{x}_2$  are homologous points if  $\mathbf{x}_2 = \mathbf{x}_1 + \mathbf{L}$ ).

The stress vector  $\mathbf{t}(\mathbf{x}) = \boldsymbol{\sigma}(\mathbf{x}) \mathbf{n}$  is also assumed to be anti-periodic (i.e.  $\mathbf{t}(\mathbf{x} + \mathbf{L}) = -\mathbf{t}(\mathbf{x})$ ).

Therefore, it can be shown that  $\mathbf{E}^0 = \langle \boldsymbol{\varepsilon} \rangle_V$ , with  $\langle \boldsymbol{\varepsilon} \rangle_V$  the mean volume deformation.

By considering the elastic law of behaviour between  $\langle \boldsymbol{\varepsilon} \rangle_V$  and  $\langle \boldsymbol{\sigma} \rangle_V$  (the mean volume stress, which is equal to the macroscopic homogenous stress tensor  $\boldsymbol{\Sigma}^0$ ), the elastic coefficients can be deduced from  $\langle \boldsymbol{\varepsilon} \rangle_V$  and  $\langle \boldsymbol{\sigma} \rangle_V$ .

When using FEM, this method is applied according to the following steps.

The REV is modelled with periodic mesh on its boundaries ( $\partial V$ ) so that each node has its homologous corresponding node on the other boundary. A displacement is then applied to the boundaries. This displacement must result in homogenous deformation  $\mathbf{E}^0$ . For instance,  $\mathbf{u}(\mathbf{x})$  is imposed on two homologous points with coordinates  $\mathbf{x}_1$  and  $\mathbf{x}_2$ .  $\mathbf{u}(\mathbf{x})$  successively takes the value  $\mathbf{L}_i$ , with  $\mathbf{L}_i$  ( $i = \{x, y, z\}$ ) having one of its components equal to the  $i^{\text{th}}$  component of the periodicity vector  $\mathbf{L}$ , and its other components equal to 0. In this case, the resulting deformation is homogenous,  $\mathbf{t}(\mathbf{x})$  is anti-periodic on boundaries and the conditions associated with (2) are respected.  $\mathbf{E}^0$  is therefore equal to unity for the considered direction. Therefore, it follows:

$$\mathbf{u}'(\mathbf{x}_2) - \mathbf{u}'(\mathbf{x}_1) = \mathbf{u}(\mathbf{x}_2) - \mathbf{u}(\mathbf{x}_1) - \mathbf{E}^0 (\mathbf{x}_2 - \mathbf{x}_1) = \mathbf{L}_i - \mathbf{E}^0 \mathbf{L}_i = \mathbf{0}, \text{ which respects the condition of periodicity for } \mathbf{u}'(\mathbf{x}).$$

Here  $\mathbf{u}(\mathbf{x}_2) - \mathbf{u}(\mathbf{x}_1)$  is taken to be equal to  $\mathbf{L}_i$  since it simplifies the computation of the elastic constants. Any values could have been considered.

The resulting macroscopic homogenous stress tensor  $\boldsymbol{\Sigma}^0$  is then computed over the volume. Finally, thanks to the elastic law of behaviour, the different equivalent elastic coefficients can be obtained on the basis of  $\boldsymbol{\Sigma}^0$  and  $\mathbf{E}^0$  (the last being equal to unity in this specific case).

For the pattern in question, the above relation  $\mathbf{u}(\mathbf{x}_2) - \mathbf{u}(\mathbf{x}_1) = \mathbf{L}_i$  is imposed as the constraint relation between the nodes of each pair of edges of the pattern. Figure 3 illustrates how the elastic constant  $E_x$  is determined with the method. The REV corresponds to the geometry previously defined in figure 2.b.

Elastic equivalent constants can be obtained for small deformation assumption. Therefore, even if large deformations are applied, their effect is not taken into account.

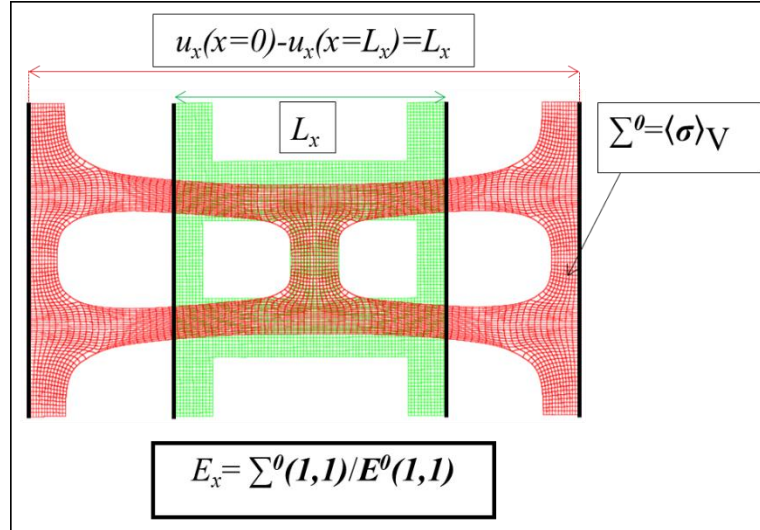


Figure 3: Elastic equivalent constant  $E_x$  with FEM

A second method aims at computing the thermal expansion coefficient. The same REV is considered with thermal loading. In this paper, the pattern is subjected to a 2D static thermal load with a thermal gradient between the gas and sodium channels (same loading as for the global method).

In a first step, a thermal model establishes the thermal field with the considered thermal loading and the mean nodal temperature is computed ( $T_{mean}$ ). This model and the resulting mean temperature can be used for the first step of the global method (see figure 1). The displacements at the boundaries of the pattern are then calculated with a thermomechanical model. As the thermal load is 2D, the mechanical model is 2D with a generalized plane strain relation. In this case:

$$\varepsilon_z = \varepsilon_z^0 = \alpha_0 \Delta T_{mean} = \alpha_0 (\Delta T_{mean} - T_{ref})$$

with  $T_{mean}$  the mean nodal temperature of the REV and  $T_{ref}$  the reference temperature used to compute thermal expansion. It should be pointed out that the mean temperature  $T_{mean}$  corresponds to same parameter as that defined in the first step of the global method (see first step in figure 1).

The applied boundary conditions correspond to the configuration of a periodic structure (*i.e.* infinite duplication of the pattern).

Figure 4 depicts the two steps and associated models for the previously defined REV.

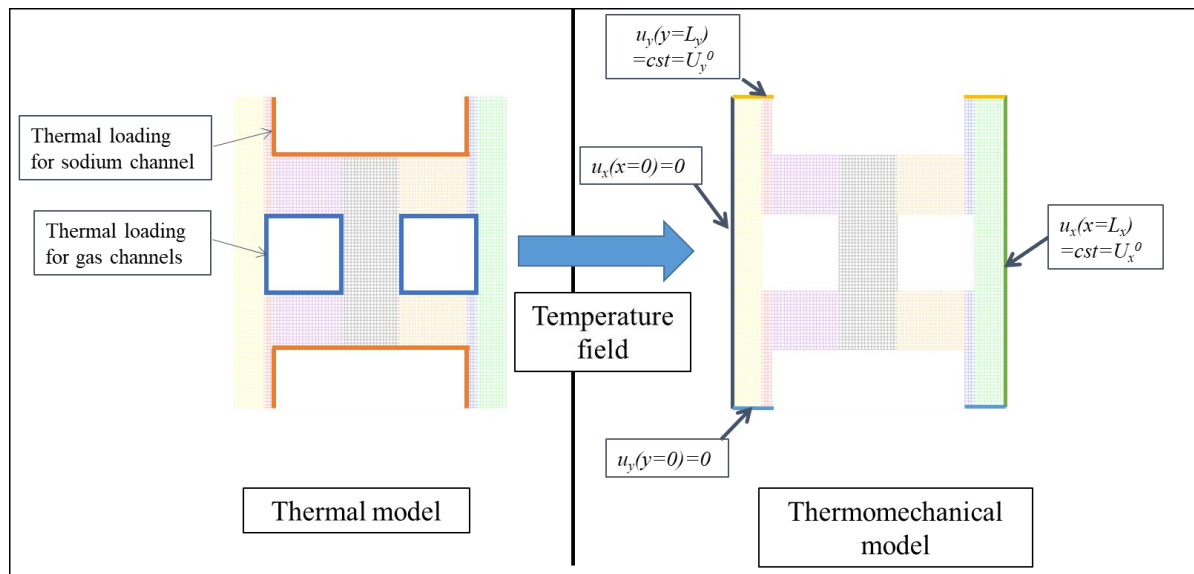


Figure 4: FEM models for computation of thermal expansion coefficient - a) Thermal model, b) Thermomechanical model

The homogenized thermal expansion coefficients are computed as follows:

$$\alpha_x = \frac{u_x(x=L_x)}{L_x \Delta T_{mean}}, \alpha_y = \frac{u_y(y=L_y)}{L_y \Delta T_{mean}}, \alpha_z = \alpha_0 \text{ (generalized plane strains assumption)}$$

$u_x(x=L_x) = U_x^0$  and  $u_y(y=L_y) = U_y^0$  are retrieved from the Finite-Element model.

The results obtained with these methods are not analysed or commented in this paper. They are simply used as input data for the global method described above. The actual values applied to the considered geometry and loading are discussed in the next section.

### 3 Assessment of the method

#### 3.1 Description

The homogenization method in question is assessed herein on the basis of two 2D cases with a periodic thermal load and a generalized plane strains assumption on the mechanical behaviour.

For each case, the resulting displacements and equivalent stress fields computed with the previous method (with EHM) are compared to those obtained with the explicit geometry, which stands as the reference.

The thermal loading involves applying temperature to both the gas and sodium channels: a temperature of 200°C is applied to the sodium channel walls whereas 0°C is applied to the gas channels, resulting in a maximum temperature difference of 200°C. As previously mentioned, a local explicit FEM model is developed to compute the thermal field and the mean temperature of the pattern. It is used to compute the thermal expansion coefficient (see Sub-section 2.2), and the mean temperature is used as input data in the first step of the global method (see figure 1).

The thermal loads applied to the pattern and the resulting thermal field in the case of periodic behaviour are presented in figure 5. An arithmetic mean function is applied using the nodal structural temperature field. A value of 100.3°C is calculated.

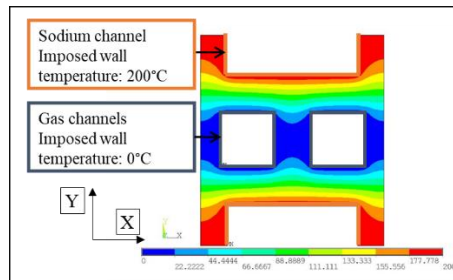


Figure 5: Pattern, applied periodic thermal loading and resulting temperature field (°C)

The method described in sub-section 2.2 is applied to compute the equivalent elastic constants. The geometry for the periodic medium (channels) is described in table 2 according to notations of figure 6. Table 3 summarises the isotropic material properties and their equivalent elastic constants (orthotropic behaviour).

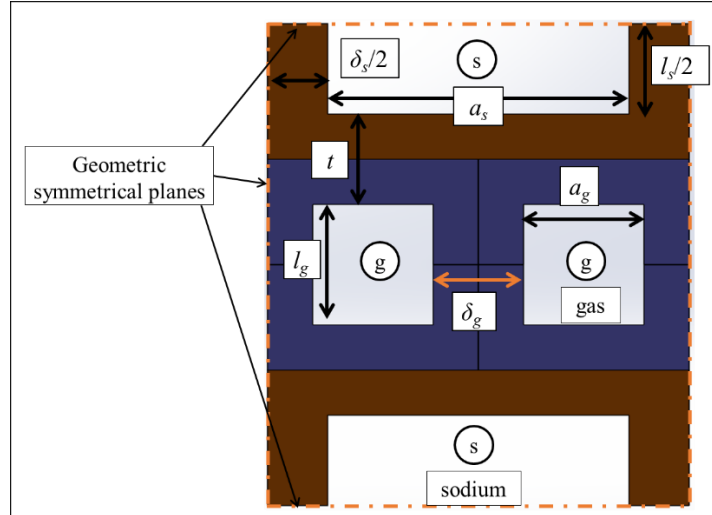


Figure 6: geometrical parameters of the channels

Table 2: geometrical parameters values of the channels and material

Material	Stainless Steel 316L	
Gas	$l_g$ (mm)	2.0
	$a_g$ (mm)	2.0
	$\delta_g$ (mm)	1.5
Sodium	$l_s$ (mm)	3.0
	$a_s$ (mm)	5.0
	$\delta_s$ (mm)	2.0
Plate	$t$ (mm)	1.5

Table 3: Isotropic material properties and equivalent elastic constants

		Isotropic material properties	Equivalent elastic constants (orthotropic behaviour)
Elastic modulus	MPa	$E_0 = 200000$	$E_x = 81998$ $E_y = 60704$ $E_z = 117858$
Shear modulus	MPa	Isotropic relation $G_0 = 76923$	$G_{xy} = 8702$ $G_{xz} = 32498$ $G_{yz} = 26542$
Poisson's ratio	-	$\nu_0 = 0.3$	$\nu_{xy} = 0.136$ $\nu_{xz} = 0.209$ $\nu_{yz} = 0.155$
Thermal expansion coefficient	m/(m.°C)	$\alpha_0 = 15.3 \cdot 10^{-6}$	$\alpha_x = 15.36 \cdot 10^{-6}$ $\alpha_y = 16.95 \cdot 10^{-6}$ $\alpha_z = 15.3 \cdot 10^{-6}$

The first case corresponds to the EHM alone with boundary conditions that reproduce infinite media (infinite periodic geometry). A finite grid of  $6 \times 6$  patterns with two symmetries and periodic boundary conditions is considered. Even if the cover plates are not present, an intermediate layer is added to the model with EHM: two layers of the explicit pattern surrounding the EHM are inserted. The geometry

and boundary conditions are depicted in figure 7 for the two models (*i.e.*, explicit model and model with EHM). In this case, it can be seen that symmetric conditions lead to the same results as periodic conditions. In addition, they result in an isostatic model. With this configuration, the behaviour of the EHM can be assessed without affecting any other parameter. It can be described as being similar to the core of the HE, far from cover plates.

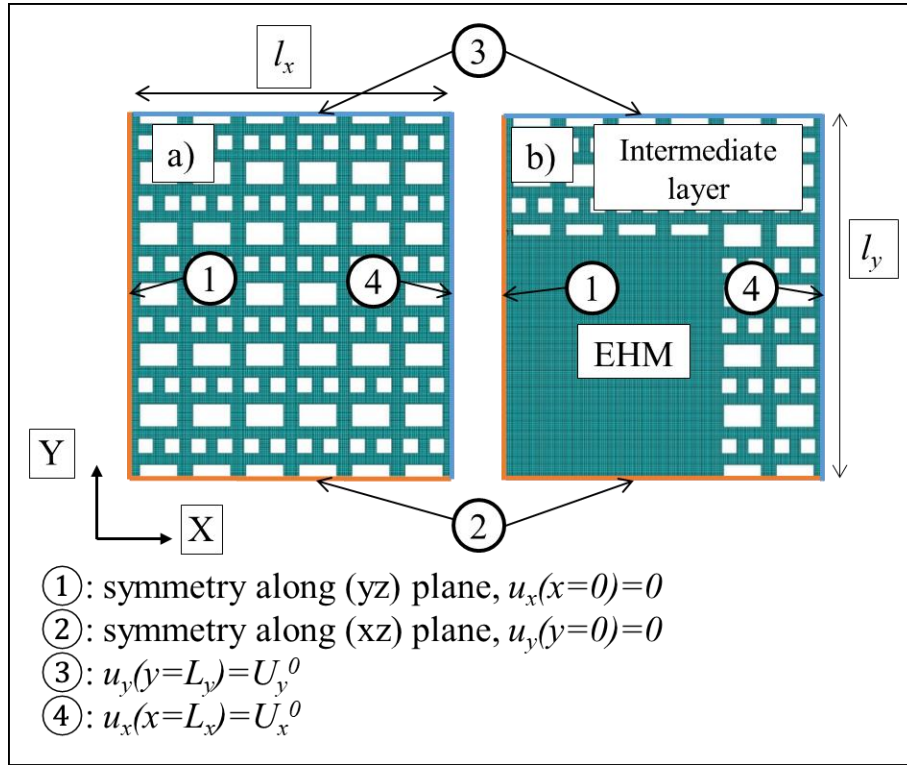


Figure 7: Case 1, 6x6 patterns with two symmetries - geometry and mechanical boundary conditions - a) Explicit geometry, b) Geometry with EHM

The second studied case takes into account a reduced but representative section of the HE: a grid of  $12 \times 12$  patterns with cover plates is considered. Due to symmetries, only a quarter of the section is modelled. The cover plates replace the periodic boundary conditions which are suppressed. Figure 8 depicts the geometry and the boundary conditions. The same thermal loading as for case 1 is applied (except for cover plates, with adiabatic conditions on their external boundaries). This model can be considered as a reduced but representative section of the HE, since the main mechanisms generating thermal stress do exist, *i.e.*, thermal gradients between channels, and thermal gradients between channels and cover plates. The results from cases 1 and 2 cannot be directly compared due to the effect of the cover plates and their own stiffness.

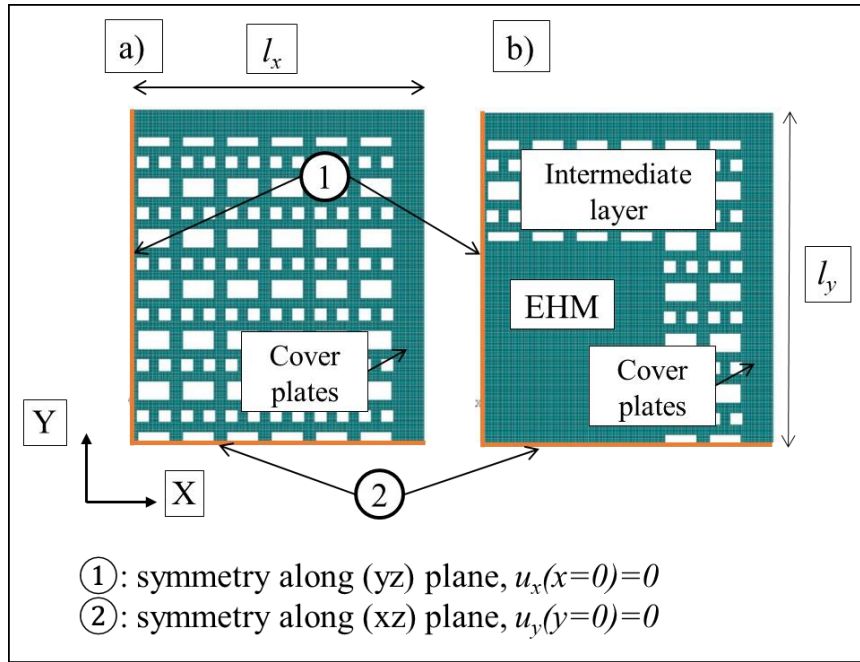


Figure 8: Case 2, 6x6 patterns with cover plates and two symmetries– geometry and mechanical boundary conditions - a) Explicit geometry; b) Geometry with EHM

The displacement components of one node on the boundaries are compared for each case. Equivalent stress (von Mises) is also compared on different lines for several patterns across the section. These patterns are identical for both cases except for case 2, in which two lines are added on the cover plates. The patterns are selected on the intermediate layer (and cover plates for case 2). The selected lines are shown in figure 9 with the following identification:

- “Pattern  $i$ ” with index  $i$  corresponding to the pattern number ( $i$  varying from 1 to 3, identical for cases 1 and 2) or “Cover Plates” corresponding to the cover plates when applicable (case 2)
- “Line  $j$ ” with index  $j$  corresponding to the line reference ( $j$  varying from 1 to 5 for a pattern or from 1 to 2 for the cover plates).

Note: the lines on cover plates do not include the full thickness. They are used only for comparison purpose. For the design of CHEs, they should cover the full thickness of the component.

The results of the EHM model are compared with those of the explicit model, which was used as the reference. A relative difference function is computed for the equivalent stress ( $S_{eqv}$ ), defined as follows:

$$Relative\ difference\ (\%) = \frac{S_{eqv}(EHM\ model) - S_{eqv}(Explicit\ model)}{S_{eqv}(Explicit\ model)} \times 100$$

The elements of both models (explicit model and model with EHM) are identical in size so that there is same number of elements for the common parts with explicit geometry. Quadratic elements are used either with 8 nodes for a quadrangular shape or with 6 nodes for a triangular shape.

After having compared the results between the two models (explicit model and model with EHM) for the two previous cases, the effect of the number of explicit patterns contained in the intermediate layer is analysed (see specific sub-section below).

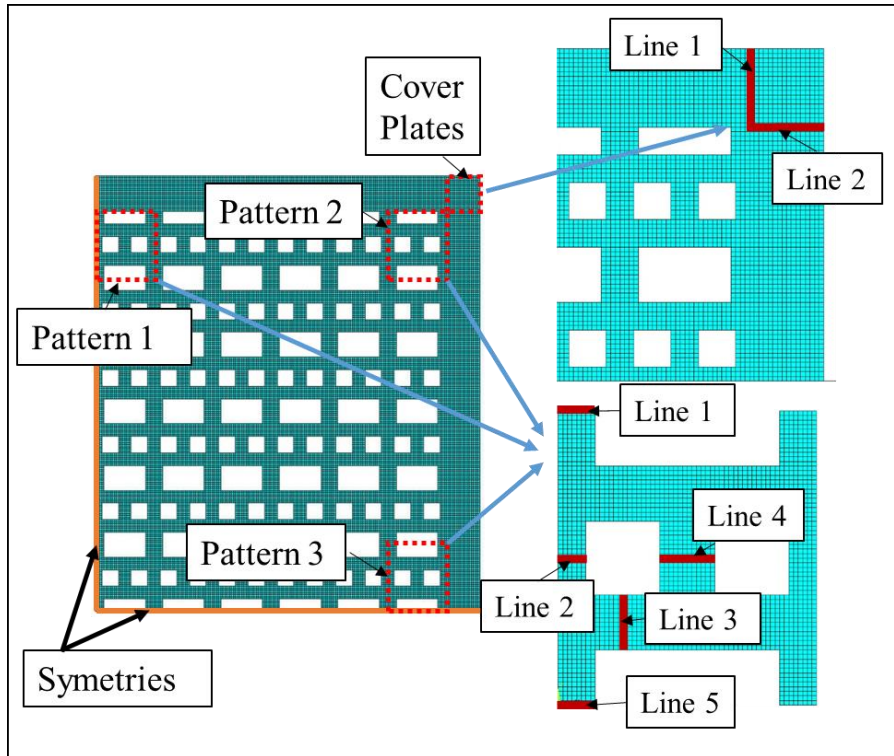


Figure 9: Selected patterns and lines for analysis of the equivalent stress (geometry corresponding to case 2)

### 3.2 Results for case 1: EHM without cover plates

The displacements and equivalent stress are post processed. The iso-values of these quantities are shown in figures 10 and 11 respectively. The same scale is applied to all iso-contour values.

The iso-contours can be seen to be qualitatively identical with respect to displacement. The displacement components are compared for nodes located on the boundaries of the model, revealing that periodic conditions lead to equal values for one component of the displacement at each frontier. For nodes located at  $x = L_x$ ,  $u_x$  value is nearly identical for both models. For nodes located at  $y = L_y$ ,  $u_y$  has the same value for both models. This result validates the equivalent properties of the EHM and especially the orthotropic thermal expansion coefficient.

The iso-contours of explicit geometry prove to be qualitatively identical with respect to equivalent stress. The maximum value over the section tends to be practically identical for both models. It should be remembered that elements are the same size in both models.

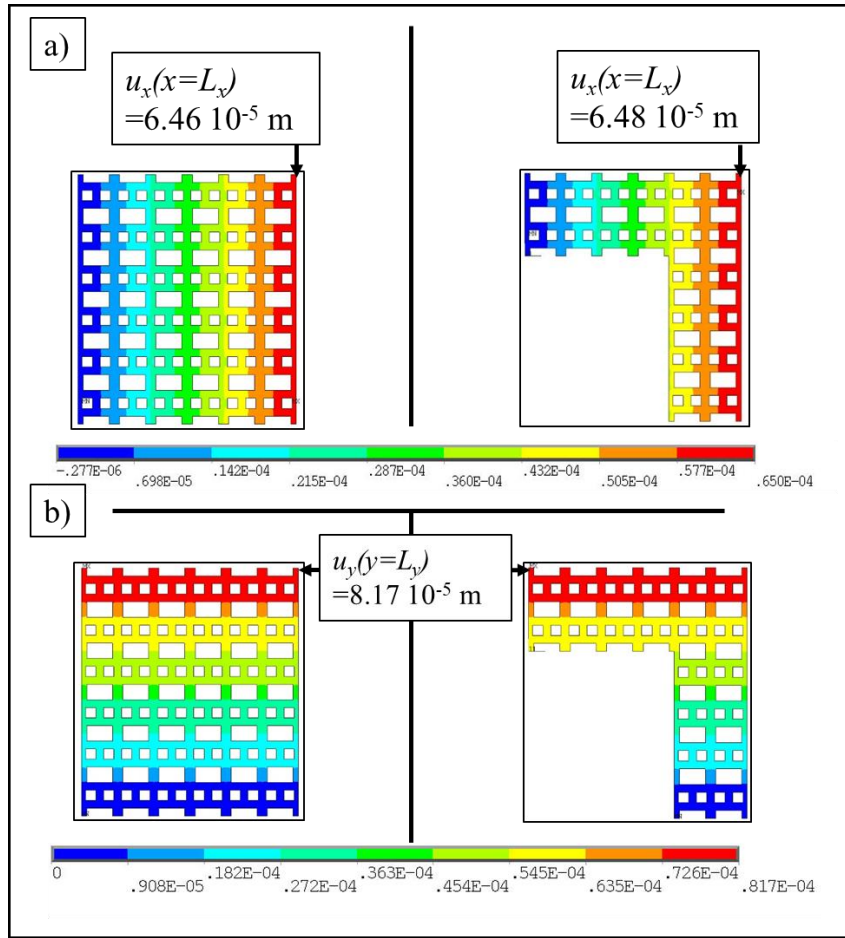


Figure 10: Case 1 – displacements (m) a)  $u_x$ ; b)  $u_y$  - Left: Explicit model; Right: EHM model (reduced to the explicit part)

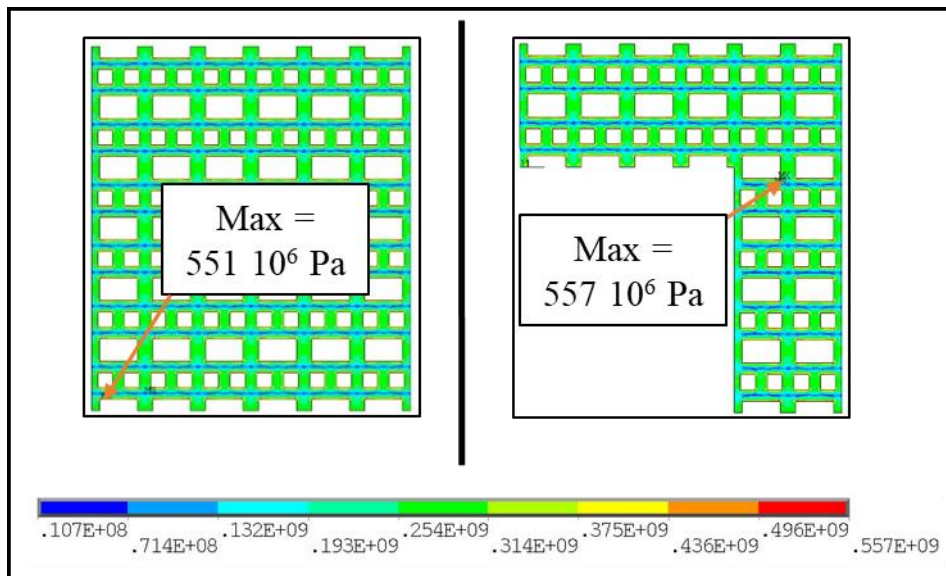
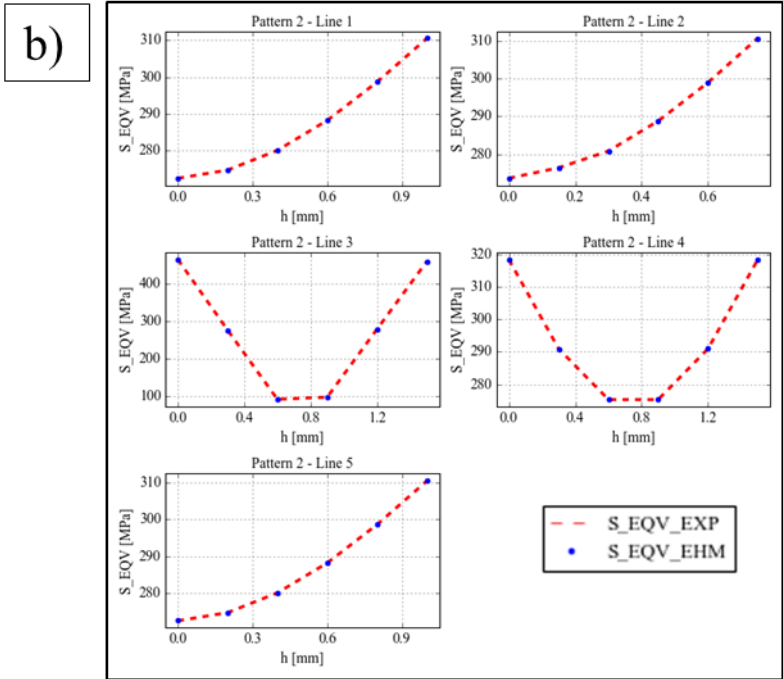
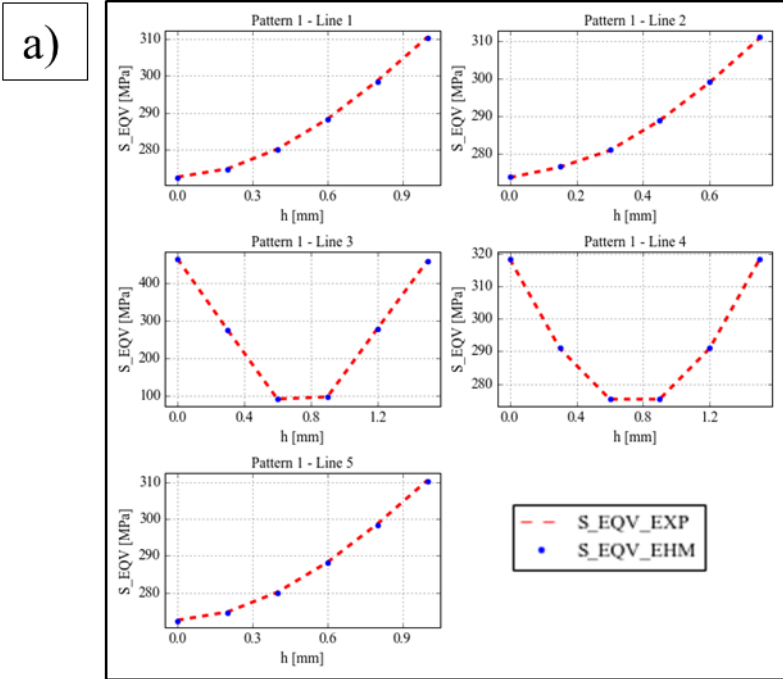


Figure 11: Case 1 – equivalent stress (von Mises, in Pa), Left: Explicit model; Right: EHM model (reduced to the explicit part)

As previously explained, the equivalent stress is quantified and compared along lines distributed on different patterns, which were defined in figure 9. The Results are given in figure 12. Qualitatively speaking, the curves are identical for both models. The relative differences are compared in table 4.

These differences are very low, with a maximum absolute value of 0.7 %, which validates the method. The maximum differences can be seen in the patterns located on the upper part of the section.



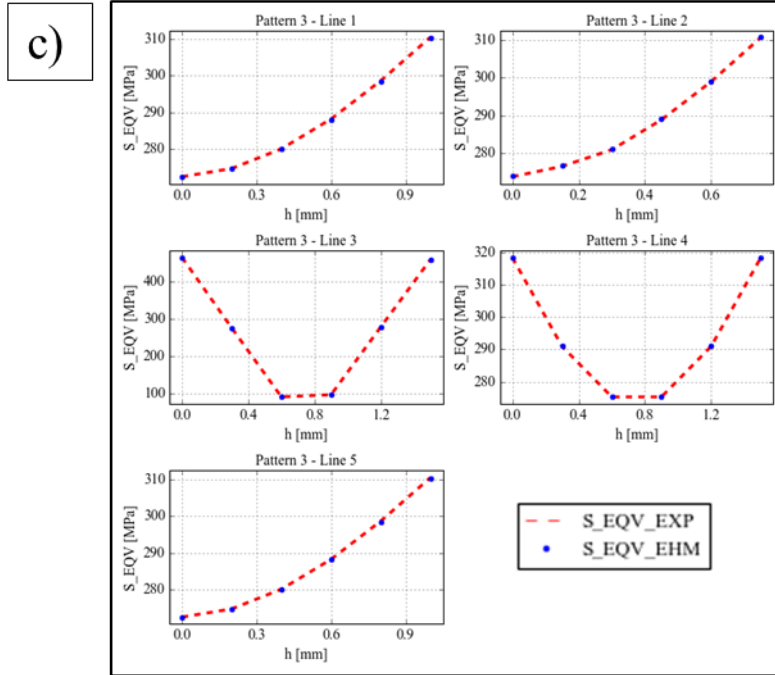


Figure 12: Case 1 - equivalent stress for selected lines on 3 patterns with *\_EXP* = explicit model, *\_EHM* = EHM model - a) Pattern 1; b) Pattern 2; c) Pattern 3

Table 4: Case 1 - relative difference for equivalent stress - EHM model vs. explicit model

Reference for pattern	Relative difference - EHM compared with explicit model	
	Max. value	Min. value
1	-0.4 %	0.5 %
2	-0.7 %	0.5 %
3	-0.1 %	0.1 %
<b>Min. / Max. over all patterns</b>	<b>-0.7 %</b>	<b>0.5 %</b>

### 3.3 Results for case 2: reduced representative section of CHE

As for case 1, the displacements and equivalent stress (von Mises) are post-processed. The iso-values of these quantities are shown in figures 13 and figure 14 respectively. The same scale is applied to all iso-contour values.

The iso-contours are proved to be qualitatively identical with respect to displacement. The displacement components are compared for the node located in the left-hand upper corner ( $x = L_x$  and  $y = L_y$ ). It can be seen that both values  $u_x$  and  $u_y$  are quasi-identical for the two models.

The iso-contours are seen to be qualitatively identical with respect to equivalent stress. The maximum value over the section is quasi-identical for both models.

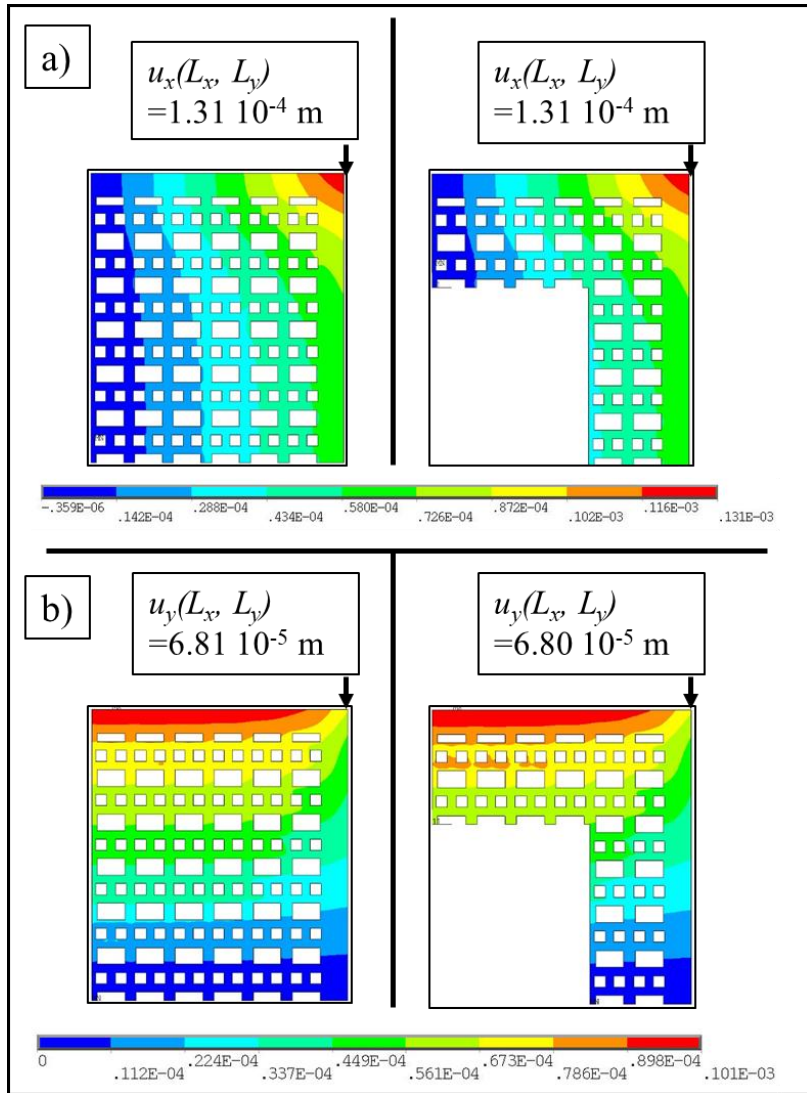


Figure 13: Case 2 – displacements (m) a)  $u_x$ ; b)  $u_y$  - Left: Explicit model; Right: EHM model, reduced to the explicit part

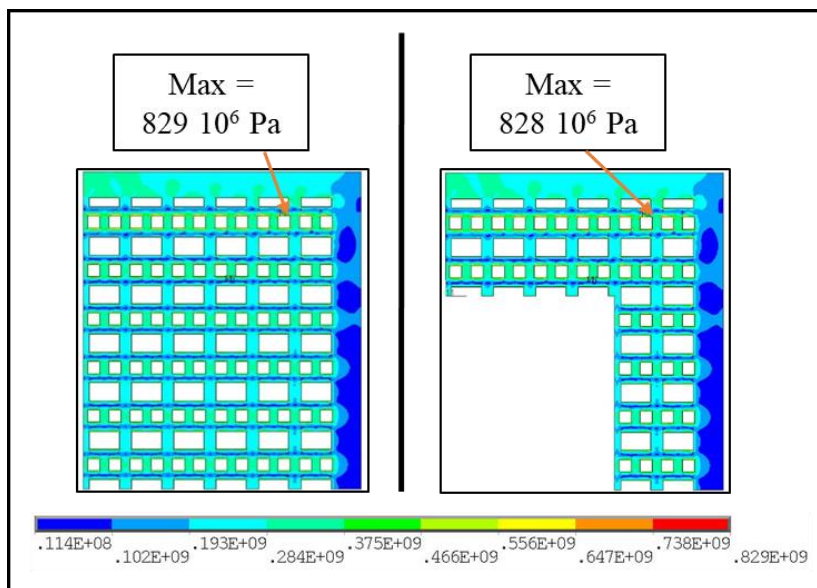
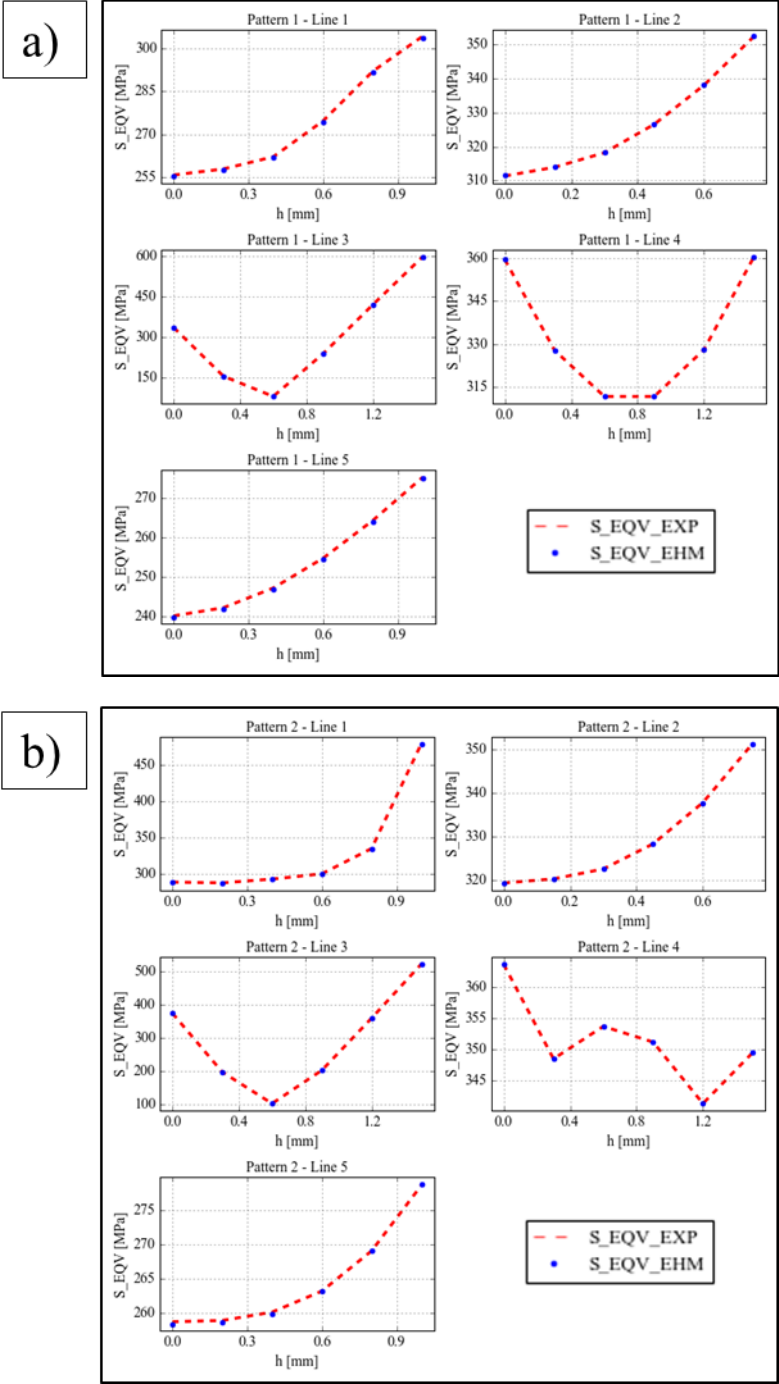


Figure 14: Case 2 – equivalent stress (von Mises, in Pa), Left: Explicit model; Right: EHM model, reduced to the explicit part

As for case 1, the equivalent stress is quantified and compared along lines distributed on different patterns, as shown in figure 9. Two lines located on the cover plates have been added (“Cover Plates - Line 1” and “Cover Plates - Line 2”). Figure 15 presents the results. Qualitatively, the curves are identical for both models. The results are not periodic as expected.

The relative differences are compared in table 5. It can be seen that they are very low with a maximum absolute value of 0.5 %, which validates the method. The maximum differences tend to exist in patterns located on the upper part of the section.

Furthermore, the values of the considered lines (figure 15) are slightly reduced compared with the results of case 1 (without cover plates, figure 12). This may be due to the suppression of the periodic boundary conditions that are applied to the model in case 1, which are replaced by the cover plates. This results in less stiff boundary conditions.



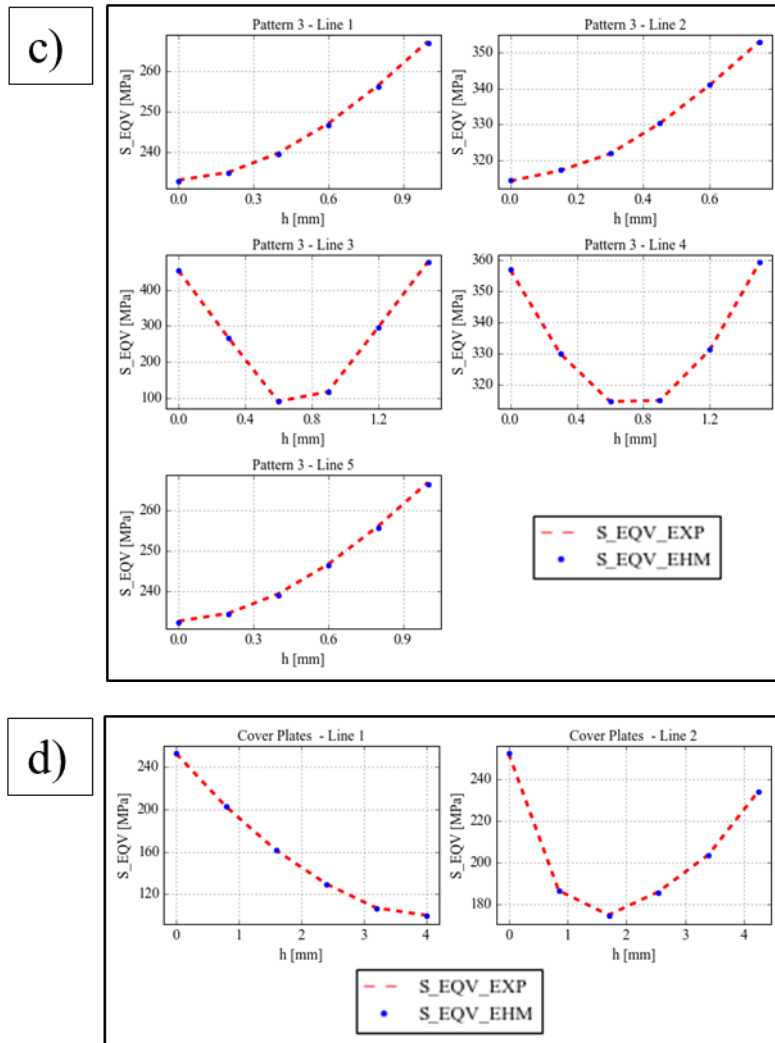


Figure 15: Case 2 - equivalent stress for selected lines on 3 patterns and cover plates with *\_EXP* = explicit model, *\_EHM* = model with EHM a) Pattern 1; b) Pattern 2; c) Pattern 3; d) Cover Plates

Table 5: Case 2 - relative difference for equivalent stress - EHM model vs. explicit model

Reference for pattern	Relative difference - EHM compared to explicit model	
	Min.	Max.
1	-0.5 %	0.0 %
2	-0.1 %	0.2 %
3	-0.2 %	0.0 %
Cover Plates	-0.1 %	0.1 %
<b>Min. / Max. over all patterns</b>	<b>-0.5 %</b>	<b>0.2 %</b>

### 3.4 Impact of the number of explicit patterns in the intermediate layer

In cases 1 and 2, two layers of explicit patterns have been modelled in the intermediate layer. This is because the number of layers may have an impact on the results and their accuracy.

Increasing the number of layers may increase the accuracy of results on the one hand, but it increases the calculation time on the other hand. Thus, these two parameters need to be optimised to obtain the best possible results.

This section discusses three cases with cover plates: the number of patterns in the intermediate layer are increased successively from one to three layers. The three geometries are shown in figure 16. The case with two layers corresponds to case 2 described above.

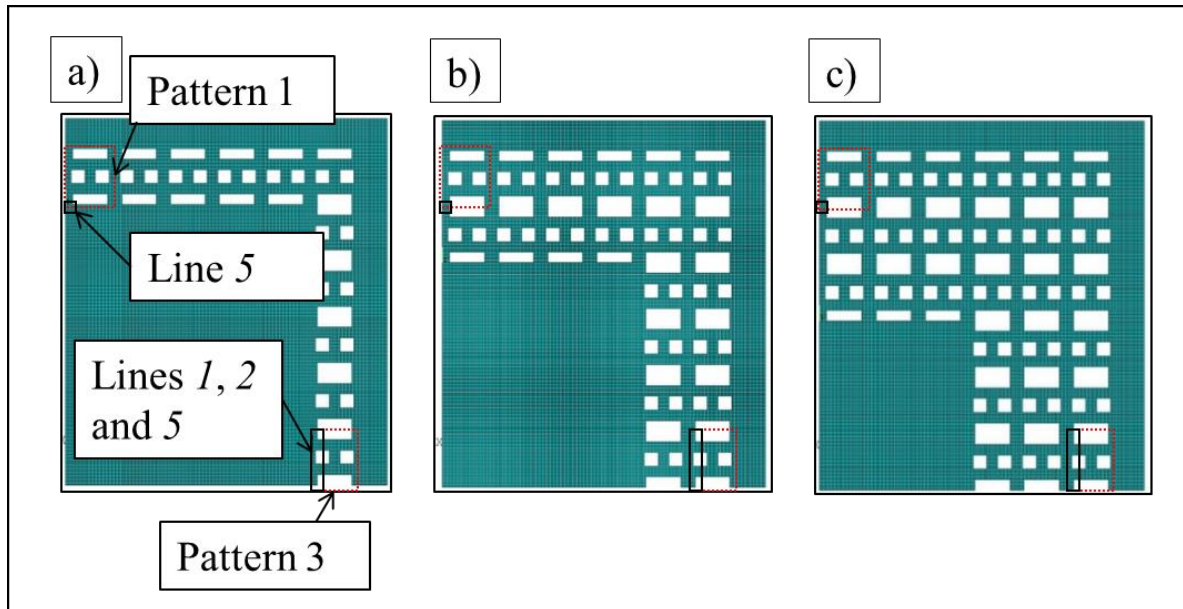


Figure 16: Geometry with a) One layer of patterns, b) Two layers of patterns, c) Three layers of patterns in the intermediate layer

The same lines as those in case 2 are analysed and the results are compared in figure 17 for patterns 1 and 3.

The results are identical for models with two and three layers, and very close to the results of the explicit model for these two models, whereas the model with one layer presents some significant differences. These differences are particularly observable for line 5 of Pattern 1, and lines 1, 2 and 5 of Pattern 3, which are located on the interface between the EHM and the intermediate layer as shown in figure 16.a. These lines underwent a sudden change in material properties (EHM / isotropic properties), which induces singularities.

The relative differences are compared in table 6. The lines located at the interface between the EHM and the intermediate layer are indicated by an asterisk (\*). The boundary between the two colours (1 %) has been selected from an engineering design perspective since lower values are considered as acceptable results. For cases with two and three layers in the intermediate layer, the differences tend to be very low with a maximum absolute value of 0.5 %. They are much higher for the model with one layer, with a maximum value of 84.4 %. The highest values can be observed for lines located at the interface with the EHM. Similar results can be observed for patterns at the interface with the EHM in the case with two and three layers (the results are not presented). Consequently, the results for lines located at the interface with the EHM or close to it are not considered representative.

As a conclusion, the results converge with an intermediate layer containing at least two layers of pattern and can directly be computed on explicit patterns that are “far enough” from the interface between the EHM and the intermediate layer (it is therefore recommended to apply one layer between the results and

the EHM). This conclusion can be extrapolated to any section size for the considered pattern, and therefore to the real CHE section. However, the effect of other parameters such as loading (effects of thermal gradients) or stiffness variation between the homogenized medium and the explicit geometry (material, channel or cover plate geometries) should be assessed.

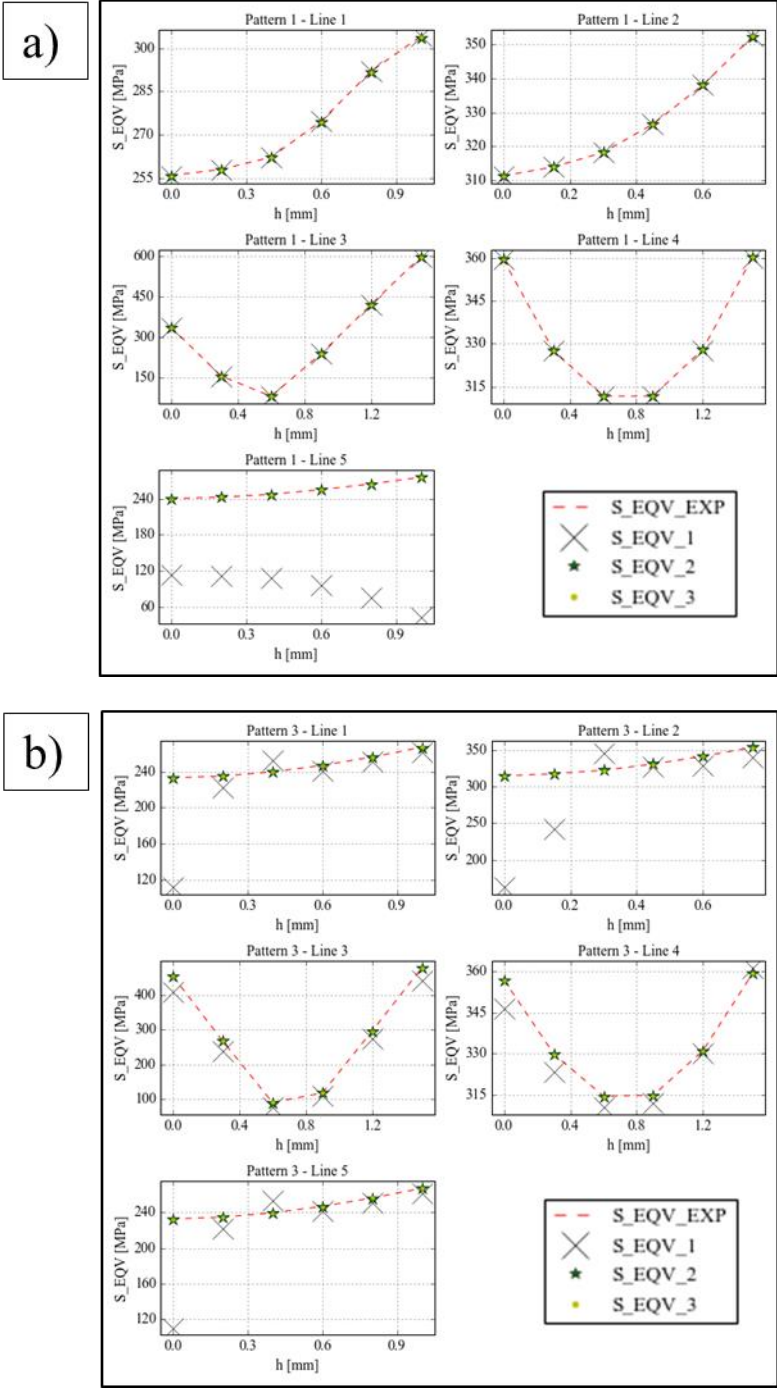


Figure 17: Comparison of the equivalent stress between three models with EHM and the intermediate layer containing one layer of patterns ( $S_{EQV\_1}$ ), two layers ( $S_{EQV\_2}$ ) and three layers ( $S_{EQV\_3}$ ), and the explicit model ( $S_{EQV\_EXP}$ ) for: a) Pattern 1; b) Pattern 3

Table 6: Relative difference for the equivalent stress computed using the EHM model with 1, 2 and 3 layers of patterns in the intermediate layer vs. the explicit model

Reference for pattern	Lines	Relative difference (absolute value, in %) - EHM compared to the explicit model – Number of layers in the intermediate layer		
		1 layer	2 layers	3 layers
1	1	0.0	0.1	0.1
	2	0.0	0.0	0.0
	3	1.0	0.5	0.4
	4	0.1	0.0	0.0
	5	84.4 *	0.1	0.1
2	1	0.4	0.1	0.0
	2	0.3	0.1	0.0
	3	2.9	0.2	0.1
	4	0.5	0.0	0.0
	5	41.3 *	0.1	0.1
3	1	52.2 *	0.1	0.0
	2	48.2 *	0.1	0.1
	3	16.2	0.2	0.1
	4	2.9	0.0	0.0
	5	52.5 *	0.1	0.0
Cover Plates	1	0.7	0.1	0.1
	2	0.4	0.1	0.1
<b>Min. / Max. over all patterns</b>		<b>84.4 %</b>	<b>0.5 %</b>	<b>0.4 %</b>

	0.0 % ≤ Difference ≤ 1.0 %
	1.0 % < Difference

## 4 Optimization - Mesh with triangular elements

Previous models have been meshed with regular quadrangles for both EHM and explicit geometries. This guarantees that there are common nodes at the interface between them and thus transmission of degrees of freedom. When convenient, this mesh is not optimized in terms of the size of the model (*i.e.* number of nodes/elements). Triangular elements can be used to reduce the size while sharing the same nodes at the interface between EHM medium and the intermediate layer. Their size can be progressively increased from the interface with the intermediate layer to the core of the EHM. Figure 18 compares the different types of mesh for models using EHM.

Contact elements can be used as an alternative to coincident nodes at the interface. Even if this method is less restrictive for meshing, it implies additional constraints during problem solving and requires more computing time. This option is not considered in this study.

In this part, the triangular mesh performances are analysed with two section sizes including cover plates (similar to case 2). The number of nodes are compared to both the explicit model and the EHM model with quadrangular elements. It is possible to validate the results by comparison of the displacement and equivalent stress.

All FE models are shown in figure 18. The first geometry corresponds to case 2 (6×6 patterns with cover plates and two symmetries, see figure 8) modified with a triangular mesh as shown in figure 18.a. The second geometry studied is identical with 4 times more patterns: 12×12 patterns with cover plates and

two symmetries (see figure 18.b). Two sizes for the EHM triangular elements are analysed for the latter geometry: the first is similar to the previous case, while the second is increased up to 3 times the initial size.

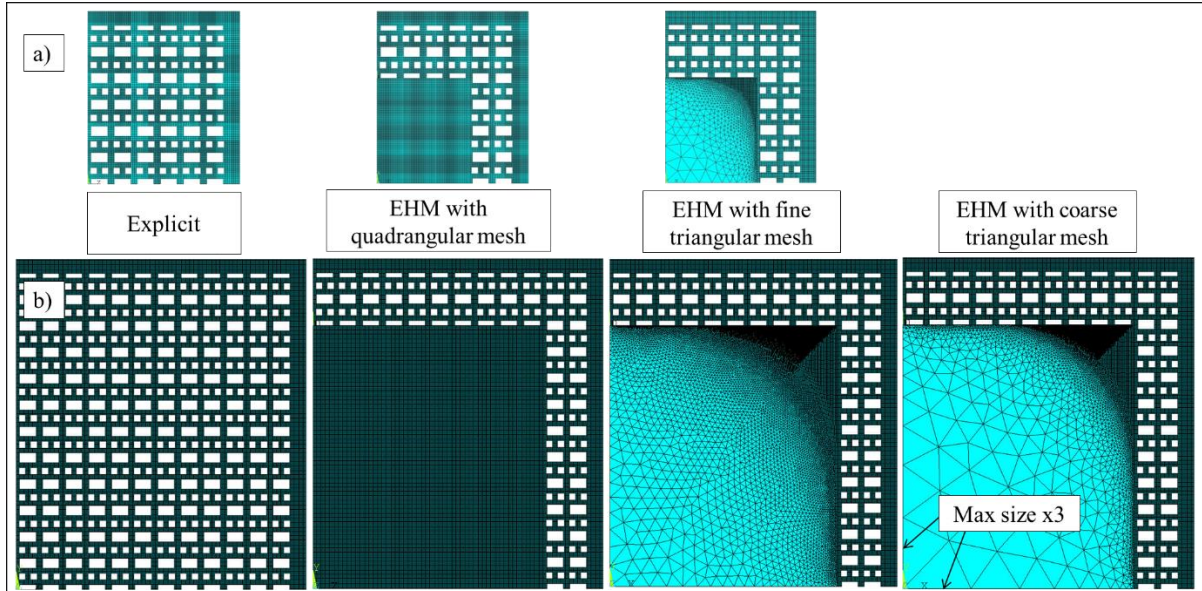


Figure 18: Geometries of the two sections with cover plates and two symmetries – a) 6×6 patterns; b) 12×12 patterns – from left to right: Explicit geometry, EHM model with quadrangular mesh, EHM models with triangular mesh (fine and coarse mesh)

Table 7 lists the number of nodes for each model. Compared to explicit model, the number of nodes is higher for the EHM model with quadrangular mesh, whereas it is lower for the EHM model with triangular mesh. Furthermore, gains are increased for the larger section with triangular mesh (from a reduction of 24 % for 6×6 patterns to 38 % for 12×12 patterns with similar size parameters for the meshing). It reaches 48 % with the coarser mesh.

As for the previous cases, the displacement and equivalent stress are post-processed. The displacement components are determined for the node located in the same position as that in case 2 (right upper corner of the section). The equivalent stress was determined for same lines as those selected for case 2.

The displacement components are quantitatively compared in table 8. The relative difference with respect to displacement can be computed as follows:

$$\text{Relative difference (\%)} = \frac{u(\text{EHM model}) - u(\text{Explicit model})}{u(\text{Explicit model})} \times 100$$

There is nearly no difference between all models.

Comparisons of the equivalent stress are given in figures 19 and 20 for the 6×6 and 12×12 sections respectively. Pattern 2 and cover plates are considered. No significant difference can be observed between the two EHM models, either with quadrangular or triangular meshes, even for the coarse triangular mesh.

The equivalent stress is compared quantitatively in table 9. The same relative differences are observed for both models using EHM. Triangular meshing does not affect the results, even for coarser mesh, whereas the size of the model is significantly reduced with respect to the explicit model. Furthermore, differences are reduced for larger section sizes, and the method can still be validated.

Table 7: Number of nodes for each model

	6×6			12×12		
	Total number of nodes	Number of nodes for EHM	Gain vs explicit	Total number of nodes	Number of nodes for EHM	Gain vs explicit
Explicit	84 361	-	-	283 987	-	-
With EHM / quadrangular mesh	97 056	43 489	+15 %	382 279	270 001	+35 %
With EHM / triangular fine mesh	64 067	10 500	-24 %	176 751	64 473	-38 %
With EHM / triangular coarse mesh	-	-	-	148 710	36 432	-48 %

Table 8: Displacement components for the node in the right upper corner of the section (in m)

	Displacements - relative difference				
	6×6		12×12		
	EHM model/ quadrangular mesh	EHM model/ triangular mesh	EHM model/ quadrangular mesh	EHM model/ fine triangular mesh	EHM model/ coarse triangular mesh
$u_x$	0.0 %	0.0 %	0.0 %	0.0 %	0.0 %
$u_y$	< 0.1 %	< 0.1 %	< 0.1 %	< 0.1 %	< 0.1 %

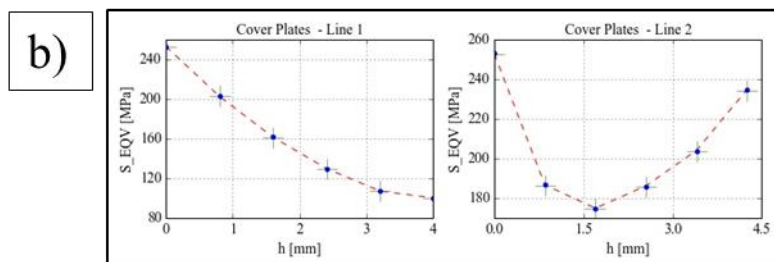
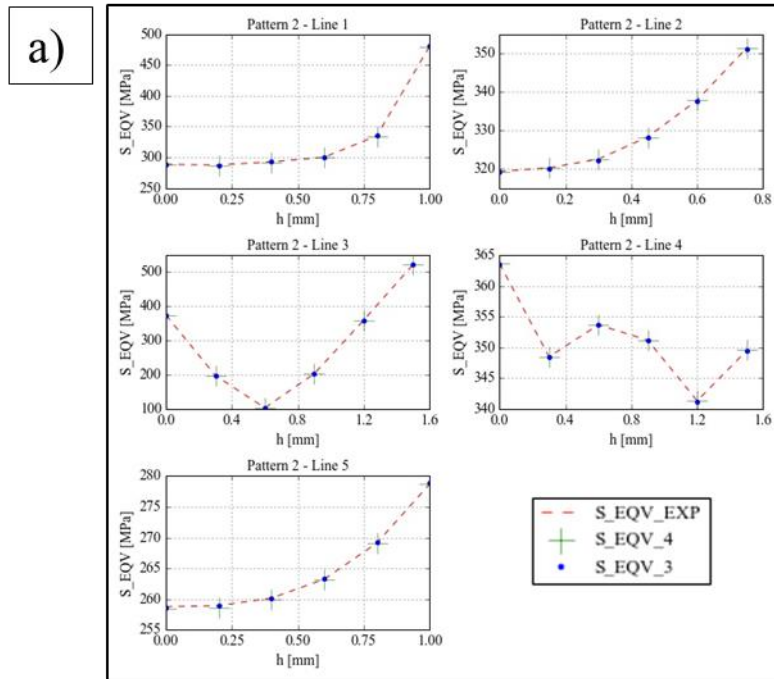


Figure 19: Section with 6×6 patterns including cover plates and two symmetries - the equivalent stress for the explicit model and EHM models with triangular mesh ( $S_{EQV\_3}$ ) and quadrangular mesh ( $S_{EQV\_4}$ ) – a) Pattern 2; b) Cover Plates

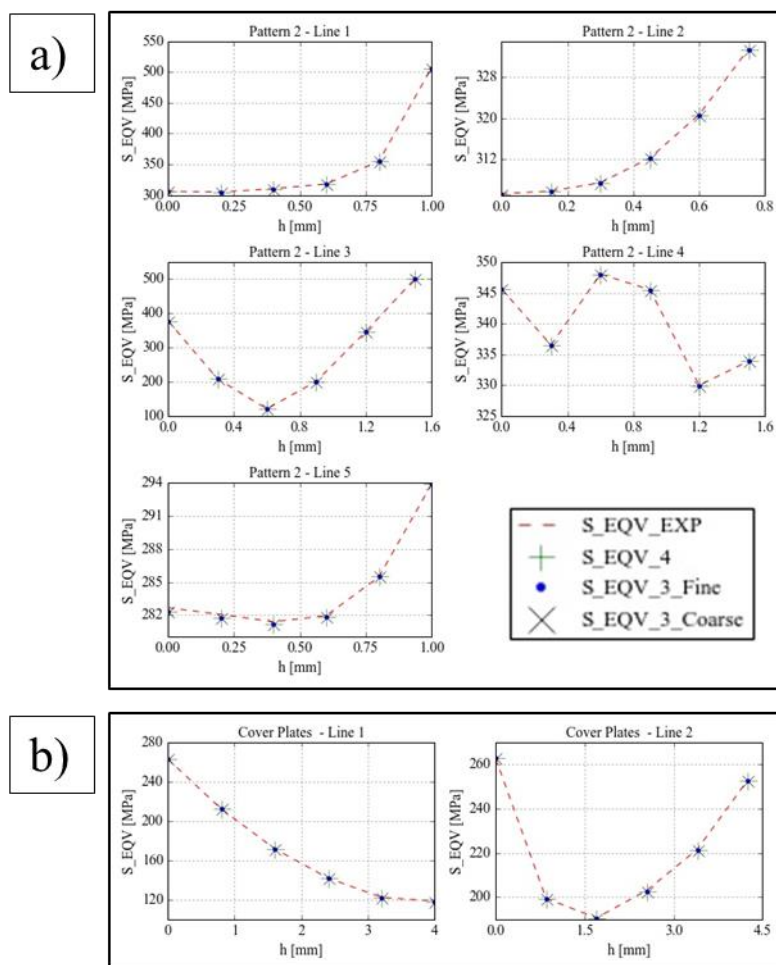


Figure 20: Section with 12×12 patterns including cover plates and two symmetries - the equivalent stress for the explicit model and EHM models with quadrangular mesh ( $S_{EQV\_4}$ ) and triangular mesh ( $S_{EQV\_3\_Fine}$ : fine mesh,  $S_{EQV\_3\_Coarse}$ : coarse mesh) – a) Pattern 2; b) Cover Plates

Table 9: Relative difference for the equivalent stress - EHM models (quadrangular and triangular meshes) vs. the explicit model

	Equivalent stress - maximum relative difference (absolute value)				
	6×6		12×12		
Reference for pattern	EHM model/ quadrangular mesh	EHM model/ triangular mesh	EHM model/ quadrangular mesh	EHM model/ fine triangular mesh	EHM model/ coarse triangular mesh
1	0.5 %	0.5 %	0.3 %	0.3 %	0.3 %
2	0.2 %	0.2 %	0.1 %	0.1 %	0.1 %
3	0.2 %	0.2 %	0.1 %	0.1 %	0.1 %
Cover Plates	0.1 %	0.1 %	0.0 %	0.0 %	0.0 %
<b>Min. / Max. over all patterns</b>	<b>0.5 %</b>	<b>0.5 %</b>	<b>0.3 %</b>	<b>0.3 %</b>	<b>0.3 %</b>

## 5 Conclusion

A method based on periodic homogeneous media has been described and assessed for the thermomechanical calculation of PCHEs under thermal loads using FE models. The Heat Exchanger core, composed of periodic channels, is modelled with equivalent homogenous medium, making it possible to reduce the number of elements. However, as an improvement of the usual method, the equivalent homogenous medium has also been coupled with an intermediate layer inserted between this part and the cover plates. This intermediate layer represents some channels with explicit geometry. This has two advantages: first, it smooths the transition between the homogenous medium and the cover plates (difference of stiffness); second, it makes it possible to directly calculate stress and strain for critical parts whereas the usual application requires using micro-macro relations to compute them on explicit geometry. The homogenous medium is defined with equivalent constants (*i.e.* the equivalent elastic constants and the orthotropic thermal expansion coefficient) which are computed separately with usual homogenization methods. Its temperature is also computed with a dedicated simple model (one channel pattern).

This method can be used to compute strain and stress of CHE under pure thermal loading. Stress and strain induced by pressure should be computed separately with a dedicated method.

The method has been assessed with a reduced but representative 2D section of a CHE. The stress calculated on the intermediate layers and on the cover plate of the model using homogenous medium has been compared with the results obtained with explicit model. A very good agreement has been found between both models with a maximum absolute relative difference of 0.5 % for the reduced but representative section with cover plates. Coupled with triangular meshing, the model with homogenous medium reduces the number of nodes compared to explicit model (up to 48 % for the considered case) with same results. It has been found that for the considered configuration, the intermediate layer should contain at least one additional layer of explicit patterns (or REV) between the EHM and the explicit channels where the results are post-processed to guarantee representative results. Finally, the efficiency and accuracy of the method have been proved with a larger section. This may extend the validity of the method to cover any size of CHE section. It has been found that the larger the section size, the greater the node reduction with triangular mesh, so that this method is of interest for large size CHEs such as those to be designed for the nuclear industry and for ASTRID.

This method has been assessed and numerically validated for 2D behaviour, as well as for both a specific and simplified thermal loading. A further validation should consist in comparing results to experiments as presented in [34] for instance. Concerning the extension of this method for 3D models, conclusions should be identical. Its application may prove particularly relevant for this type of geometry under transient thermal loadings requiring lengthy computational times, even if its reliability for transient simulation is still to be assessed. Moreover, 3D thermal loadings can also be applied which may increase thermal stress. Thermal loads not only result from the related temperature difference between the two fluids (thermal gradient between the channels), but also from possible flow distribution differences across the cross section, from thermal differences between the two HE sides (inlet and outlet when considering one fluid) under normal operating conditions, and from transient thermal loads (*e.g.* thermal shock). These spatially complex loads can be taken into account using this method.

The stress and strain computed on explicit channels (critical parts) can be analysed in order to verify the compliance with rules according to the applied design code. This method can be used to design PCHEs or any other heat exchanger technologies under thermal loading as long as the channel arrangement shows periodicity.

## Funding sources

This study was supported by the CEA Generation IV programme.

## Acknowledgments-Author contributions

Christophe Garnier: methodology, original draft and editing

Sébastien Vincent: review and proof reading

Pierre Lamagnère: review and proof reading

Yves Lejeail: review

Lionel Cachon: proof reading, conceptualization

## Declarations of interest

Declarations of interest: none.

## References

- [1] Chai L., Tassou S.A., A review of printed circuit heat exchangers for helium and supercritical CO<sub>2</sub> Brayton cycles. *Thermal Science and Engineering Progress*, 2020, 18(100543).
- [2] Aakre S.R., Anderson M.H., Molten salt to supercritical CO<sub>2</sub> diffusion-bonded heat exchanger testing to support component certification for advanced nuclear power systems. 18<sup>th</sup> International Topical Meeting on Nuclear Reactor Thermal Hydraulics, NURETH 2019, 2019, 4876-4887.
- [3] Cheng K., Huai X., Guo J., Sun X., Experimental study of thermal-hydraulic performance of a printed circuit heat exchanger. 18<sup>th</sup> International Topical Meeting on Nuclear Reactor Thermal Hydraulics, NURETH 2019, 2019, 688-700.
- [4] Sabharwall P., Clark D., Glazoff M., Zheng G., Sridharan K., Anderson M., Advanced heat exchanger development for molten salts. *Nuclear Engineering and Design*, 2014, 280: 42-56.
- [5] Cachon L., Vitillo F., Garnier Ch., Jeanningros X., Rigal E., Le Bourdais F., Madeleine S., Gastaldi O., Laffont G., Status of the Sodium Gas Heat Exchanger (SGHE) development for the Nitrogen Power Conversion System planned for the ASTRID SFR prototype. *Proceedings of ICAPP 2015, May 2015 - Nice (France)*, 2015.
- [6] Plancq D., Cachon L., Woaye Hune A., Verpoest Th., Progress in the ASTRID Sodium Gas Heat Exchanger development. *International Conference on Fast Reactors and Related Fuel Cycles: Next Generation Nuclear Systems for Sustainable Development (FR17)*, Yekaterinburg, Russian Federation, 2017.
- [7] Plancq D., Cachon L., Remy A., Quenaut J., Fasel Y., Gama P., Dauphin A., Raquin L., Status of the ASTRID gas power conversion system option. *GIF Symposium 2018 - The Generation IV International Forum*, Paris, October 2018.
- [8] Simanjuntak A. P., Lee J. Y., Mechanical Integrity Analysis of a Printed Circuit Heat Exchanger with Channel Misalignment. *Applied Sciences*, 2020, 10(2169).
- [9] Lee Y., Lee J.I., Structural assessment of intermediate printed circuit heat exchanger for sodium-cooled fast reactor with supercritical CO<sub>2</sub> cycle. *Annals of Nuclear Energy*, 2014, 73: 84-95.
- [10] De la Torre R., François J.-L., Lin C.-X., Assessment of the design effects on the structural performance of the Printed Circuit Heat Exchanger under very high temperature condition. *Nuclear Engineering and Design*, 2020, 365(110713).
- [11] Park C.-G., Kim H.-W., Cho J.H., Kim J.-B., Kim S.-K., Structural Design and Evaluation of a Steam Generator in PGSFR. *International Conference on Fast Reactors and Related Fuel Cycles: Next Generation Nuclear Systems for Sustainable Development*, report number IAEA-CN245-162, 2017.
- [12] Wu J., Yao S., Zhao Z., Xiao Q., Ke Z., Lin Y., Thermal stress analysis of printed circuit heat exchanger based on thermal-structural coupling method. *IOP Publishing, Conference series Materials Science and Engineering*, 2020, 721(012034).
- [13] Bornert M., Bretheau T., Gilormini P., *Homogénéisation en mécanique des matériaux 1 – Matériaux aléatoires élastiques et milieux périodiques*, Hermes Science Publication, 2001.

- [14] Charollais F., Bauer M., Coster M., Jeulin D., Troabas M., Modelling the structure of a nuclear ceramic obtained by solid phase sintering. *Acta Stereologica*, 1997, 16: 315-321.
- [15] Onimus F., Bechade J.L., A polycrystalline modelling of the mechanical behaviour of neutron irradiated zirconium alloys. *Journal of Nuclear Materials*, 2009, 384.
- [16] Jeulin D., Modèles morphologique de structures aléatoire et de changement d'échelle, Université de Caen, 1991.
- [17] Jeulin D., Proceedings of the Symposium on the Advances in the Theory and Applications of Random Sets, World Scientific Publishing Company, Singapore, 1997.
- [18] El Abdi A., Castelier E., Bouloré A., Michel J.-C., Lantuéjoul C. and al., Génération de microstructures de combustible nucléaire hétérogène et homogénéisation mécanique. Colloque national Mécamat "Matériaux Numériques", January 2018.
- [19] Cartaud P., Messenger T., Computational homogenization of periodic beam-like structures. *International Journal of Solids and Structures*, 2006, 43: 686-696.
- [20] Lewiński T., Homogenizing stiffnesses of plates with periodic structure. *International Journal of Solids and Structures*, 1992, 29: 309-326.
- [21] Gonella S., Ruzzene M., Homogenization and equivalent in-plane properties of two-dimensional periodic lattices. *International Journal of Solids and Structures*, 2008, 45: 2897-2915.
- [22] Brockenborough J.R., Sureh S., Wienecke H.A., Deformation of metal matrix composites with continuous fibers: geometrical effects of fiber distribution and shape. *Acta Metallurgica Materialia*, 1991, 39: 735-752.
- [23] Pastor J., Ohayon J., Disdier C., Homogénéisation périodique et composites à fibres actives, *Compte rendu, Académie des Sciences Paris*, t. 326, Série II b, Mécanique des solides et des structures, 1998.
- [24] Gornet L., Marckmann G., Lombard M., Détermination des coefficients d'élasticité et de rupture d'âmes nids d'abeilles Nomex®: Homogénéisation périodique et simulation numérique. *Mechanics & Industry*, 2005, 6(6): 595-604.
- [25] Di Paola F., Modélisation multi-échelles du comportement thermo-élastique de composites à particules sphériques, Ecole Centrale Paris, 2010.
- [26] Castelier E., Homogenization of one dimensional SiC/SiC composites in traction condition, *ICFRM2007/132*, 2007.
- [27] Rohmer E., Couégnat G., Caty O., Lorette C., Modelling the mechanical properties of SiCf/SiC. 17<sup>èmes</sup> Journées Nationales sur les Composites (JNC17), Poitiers-Futuroscope, France, June 2011.
- [28] Chateau C., Gélébart L., Bornert M., Multiscale approach of mechanical behaviour of Sic/Sic composites: elastic behaviour at the scale of the tow. *Technische Mechanik*, 2010, 30.
- [29] Ge L., Jiang W., Zhang Y., Tu S.-T., Analytical evaluation of the homogenized elastic constants of plate-fin structures. *International Journal of Mechanical Sciences*, 2017, 134: 51-62.
- [30] Xu X. F., Qiao P., Homogenized elastic properties of honeycomb sandwich with skin effect. *International Journal of Solids and Structures*, 2002, 39: 2153-2188.
- [31] Dirrenberger J., Forest S., Simulation et homogénéisation de microstructures périodiques, Centre des Matériaux, Mines ParisTech, 2010.
- [32] Tsuda M., Takemura E., Asada T., Ohno N., Igari T., Homogenized elastic–viscoplastic behaviour of plate-fin structures at high temperatures: Numerical analysis and macroscopic constitutive modelling. *International Journal of Mechanical Sciences*, 2010, 52: 648-656.
- [33] Tsuda M., Ohno N., Duplex model for homogenized elastic–viscoplastic behavior of plate–fin. *International Journal of Plasticity*, 2011, 27: 1560-1576.
- [34] Mizokami Y., Igari T., Kawashima F., Sakakibara N., Tanihira M., Yuhara T., Hiroe T., Development of structural design procedure of plate-fin heat exchanger for HTGR. *Nuclear Engineering and Design*, 2013, 255: 248-262.
- [35] Ge L., Jiang W., Wang Y., Tu S.-T., Creep-fatigue strength design of plate-fin heat exchanger by a homogeneous method. *International Journal of Mechanical Sciences*, 2018, 146-147: 221-233.
- [36] Jiang W., Ge L., Zhang Y., Gong J., Tu S., Xie X, Method for creep-fatigue strength of plate-fin heat exchanger, Patent No. US 10289772 B2 from May 2019.
- [37] Planel O., Brisson S., Homogenization Method: A Way to Improve Finite Element Analysis on Brazed Heat Exchangers. Conference SAE 2004 World Congress & Exhibition, 2004.